

# GPU parallelization of a hybrid pseudospectral fluid turbulence framework using CUDA

Duane Rosenberg<sup>a</sup>, Pablo D. Mininni<sup>b</sup>, Raghu Reddy<sup>c</sup>, Annick Pouquet<sup>d,e</sup>

<sup>a</sup>1401 Bradley Drive, Boulder, CO 80305

<sup>b</sup>Departamento de Física, Facultad de Ciencias Exactas y Naturales & IFIBA, CONICET, Ciudad Universitaria, 1428 Buenos Aires, Argentina

<sup>c</sup>CSRA Inc., at NOAA/NWS/NCEP/Environmental Modeling Center, 5830 University Research Court, Suite 2146 College Park, MD 20740 USA

<sup>d</sup>National Center for Atmospheric Research, P.O. Box 3000, Boulder, CO 80307

<sup>e</sup>Laboratory for Atmospheric and Space Physics, CU, Boulder, CO 80309-256 USA

---

## Abstract

An existing hybrid MPI-OpenMP scheme is augmented with a CUDA-based fine grain parallelization approach for multidimensional distributed Fourier transforms, in a well-characterized pseudospectral fluid turbulence code. Basics of the hybrid scheme are reviewed, and heuristics provided to show a potential benefit of the CUDA implementation. The method draws heavily on the CUDA runtime library to handle memory management, and on the cuFFT library for computing local FFTs. The manner in which the interfaces are constructed to these libraries, and ISO bindings utilized to facilitate platform portability, are discussed. CUDA streams are implemented to overlap data transfer with cuFFT computation. Testing with a baseline solver demonstrates significant aggregate speed-up over the hybrid MPI-OpenMP solver by offloading to GPUs on an NVLink-based test system. While the batch streamed approach provides little benefit with NVLink, we see a performance gain of 30% when tuned for the optimal number of streams on a PCIe-based system. It is found that strong GPU scaling is ideal, or slightly better than ideal, in all cases. In addition to speed-up measurements for the fiducial solver, we also consider several other solvers with different numbers of transform operations and find that aggregate speed-ups are nearly constant for all solvers.

*Keywords:* Computational fluids, Numerical simulation, MPI, OpenMP, CUDA, Parallel scalability

---

## 1. Introduction

Turbulent flows and multi-scale interactions are often studied computationally using the pseudospectral numerical method (Orszag, 1972; Canuto et al., 1988). This is because of its inherent high order truncation, its consequent lack of diffusivity and dispersion and, importantly, because of its local (per node) computational complexity, which, using fast spectral transforms at a linear grid resolution of  $N$ , goes as  $N \log N$  instead of  $N^2$ . The grid resolutions required to study turbulent flows—without resorting to modeling—vary as a high power of the Reynolds number that characterizes the turbulence. For geophysical fluids with Reynolds numbers often larger than  $10^8$ , this can translate into grids with more than  $10^{18}$  gridpoints in three dimensions, yielding a truly exascale computation. For this reason, even when lower Reynolds numbers are considered, computational fluid dynamics (CFD) approaches to turbulence require efficient parallelization methods with good scalability up to very large number of processors.

In Mininni et al. (2011) (hereafter, **M11**) we presented a hybrid MPI-OpenMP pseudospectral method and showed its scalability and parallel efficiency up to reasonably high core counts. We also provided guidance on optimization on NUMA systems which touched on issues of MPI task and thread affinity to avoid resource contention. The present paper builds upon this previous study. It was recognized early that we could achieve significant performance gains if we could essentially eliminate the cost of local Fast Fourier Transforms (FFTs) and perhaps other computations by offloading this work to an accelerator. The CUDA FFT library (NVIDIA, 2018b) together with the CUDA runtime library (NVIDIA, 2018a) allow us to do this. The idea is straightforward: copy the data to the device, compute the local transform and perhaps other local calculations, and copy back so that communication and additional computation may be carried out.

Because of the sheer number of applications and because of the desire to reach higher Reynolds numbers and larger and more complex computational domains, fluid and gas dynamics applications have often been at the forefront

of development for new computational technology. The most successful of these efforts for accelerators have generally been particle-based or particle-like methods that are known to scale well and have been ported to GPU-based systems (Ripesi et al., 2014; Yokota et al., 2013), and even to Cell processor-based systems (Stürmer et al., 2009). It is not uncommon, however, to find even with ostensibly highly scalable methods that reported performance measurements are restricted to single nodes or even to single kernels on a single accelerator rather than to holistic performance. On the other hand, global modeling efforts have shown superb aggregate performance on GPU-based systems (Govett et al., 2017), but such codes often used for numerical weather or climate are typically low-order, and not suited for studies of detailed scale interactions.

While there are some efforts in the literature to port pseudospectral methods to GPUs (see, e.g., Thibault and Senocak, 2009), most appear to be tailored to smaller accelerated desktop solutions that avoid the issue of network communication that necessarily arises in massively distributed applications of the method (see Sec. 2). This communication is usually considered such a severe limitation (Yokota et al., 2013) that it has repeatedly sounded the death knell for pseudospectral methods for some time, reputedly preventing scaling to large node counts and yielding poor parallel efficiency in multi-node CPU- and GPU-based systems. This may eventually be borne out; however, as demonstrated in **M11** and in subsequent work (Rosenberg et al., 2015), our basic hybrid scheme continues to scale on CPU-based multicore systems with good parallel efficiency, likely due in part to the 1D domain decomposition scheme that is used (Sec. 2). Indeed, other authors (Dmitruk et al., 2001; Kaneda et al., 2003; Yeung et al., 2005; Donzis et al., 2008; Chatterjee et al., 2018) have also seen good scaling of pseudospectral methods using alternative decompositions. As we will see below, good scaling is expected to continue on emerging GPU-based systems with our new CUDA implementation.

In this paper we present a new method based on the hybrid algorithm originally discussed in **M11** that allows us to run on GPUs. The problem is formulated and given context in Sec. 2, where we also update the formulation in **M11** to accommodate anisotropic grids. In Sec. 3 the implementation of the method is discussed, showing how the interfaces to the CUDA runtime and cuFFT libraries are handled, as well as how portability is maintained. Results showing the efficacy of the CUDA implementation on *total* runtimes are provided in Sec. 4 for our reference equations, and aggregate speed-ups for other solvers are also presented. We establish that the transfer time to and from the device becomes a new cost that can lessen the gains achieved by computing on the GPUs, and we show how CUDA streams may be used to diminish the impact of the transfer on different systems. Finally, in Sec. 5 we offer our conclusions, as well as some observations about the code and future work. Overall, the method we present gives significant speed-ups on GPUs, ideal or better than ideal parallel scaling when multiple nodes and GPUs are used, and can be used to generate fast parallel implementations of FFTs, or three-level (MPI-OpenMP-CUDA) parallelizations of pseudospectral CFD codes, or of other CFD methods requiring all-to-all communication.

## 2. Problem description

Our motivation is to solve systems of partial differential equations (PDEs) that describe fluids in periodic Cartesian domains for purposes of investigating turbulent interactions at all resolvable scales. A prototypical system of PDEs that describes the conservation of momentum of an incompressible fluid in a stably stratified domain is given by the Boussinesq equations:

$$\partial_t \mathbf{u} + \nabla p + \mathbf{u} \cdot \nabla \mathbf{u} = -N_{bv} \theta \hat{z} + \nu \Delta \mathbf{u}, \quad (1)$$

$$\partial_t \theta + \mathbf{u} \cdot \nabla \theta = N_{bv} w + \kappa \Delta \theta, \quad (2)$$

$$\nabla \cdot \mathbf{u} = 0, \quad (3)$$

in which  $\mathbf{u}$  is the velocity,  $p$  the pressure (effectively a Lagrange multiplier used to satisfy the incompressibility constraint given by Eq. 3),  $\theta$  the temperature (or density) fluctuations, and  $N_{bv}$  is the Brunt-Väisälä frequency which establishes the magnitude of the background stratification. The dissipation terms are governed by the viscosity  $\nu$ , and the scalar diffusivity  $\kappa$ . These equations, essentially the incompressible Navier-Stokes equations together with an active scalar (the temperature) and additional source terms, are relevant for studies of geophysical turbulence, and in the following will be considered as our reference equations for most tests.

We will also consider three other systems of PDEs often used for turbulence investigations in different physical contexts, of similar form except for the last case relevant for condensed matter physics. When in the equations

above the temperature is set to zero ( $\theta = 0$ ), we are only left with the incompressible Navier-Stokes equations, given by Eq. 1 and Eq. 3. This set of equations is used to study hydrodynamic (HD) turbulent flows. In space physics magnetohydrodynamic (MHD) flows are often considered, which describe the evolution of the velocity field  $\mathbf{u}$  and of a magnetic field  $\mathbf{B}$ :

$$\partial_t \mathbf{u} + \nabla p + \mathbf{u} \cdot \nabla \mathbf{u} = \mathbf{B} \cdot \nabla \mathbf{B} + \nu \Delta \mathbf{u}, \quad (4)$$

$$\partial_t \mathbf{B} - \nabla \times (\mathbf{v} \times \mathbf{B}) = \eta \Delta \mathbf{B}, \quad (5)$$

$$\nabla \cdot \mathbf{u} = \nabla \cdot \mathbf{B} = 0, \quad (6)$$

where  $\eta$  is the magnetic diffusivity. Finally, to study quantum turbulence the Gross-Pitaevskii equation (GPE) describes the evolution of a complex wavefunction  $\psi$ :

$$i\hbar \partial_t \psi = -\hbar^2 / (2m) \Delta \psi + g |\psi|^2 \psi, \quad (7)$$

where  $g$  is a scattering length and  $m$  a mass. The four sets of equations (Boussinesq, HD, MHD, and GPE) allow us to explore the performance of the method for different equations often used in CFD applications.

Our work relies on the Geophysical High Order Suite for Turbulence (GHOST) code (**M11**), which provides a framework for solving these types of PDEs using a pseudospectral method (Patterson and Orszag, 1971; Gottlieb et al., 1984; Canuto et al., 1988). To discretize the PDE, in general, each component of the fields is expanded in terms of a discrete Fourier transform of the form

$$\hat{\phi}_{pqr} = \sum_{i=j=k=0}^{N_x-1, N_y-1, N_z-1} \phi_{ijk} \exp[-2\pi i(pL_x/N_x + qL_y/N_y + rL_z/N_z)], \quad (8)$$

where  $\hat{\phi}_{pqr}$ , represent the (complex) expansion coefficients in spectral space. We focus here on 3D transforms, and neglect any normalization. The expansion above represents the *forward* Fourier transform; a similar equation holds for the *backward* transform but with a sign change in the exponential (again, neglecting any normalization). The indices  $(i, j, k)$  represent the physical space grid point, and  $(p, q, r)$  represent the wave number grid location. Note that both the physical box size,  $L_i$ , and the number of physical space points,  $N_i$ , may be specified independently in each direction in our implementation enabling non-isotropic expansions in the  $(L_x, L_y, L_z)$  domain. This is a major difference between the current algorithm and the version discussed in **M11** (Sojovolosky et al., 2018).

Taking the continuous Fourier transform and utilizing the discrete expansion given by Eq. 8 in the system of PDEs, yields a system of time-dependent ordinary differential equations (ODEs) in terms of the complex Fourier coefficients,  $\hat{\phi}_{pqr}$ , for each field component. These represent the solution at a point (or *mode*) in the associated 3D spectral space. In GHOST, the system of ODEs is solved using an explicit Runge-Kutta scheme (of 2nd-4th order); explicit time stepping is used to resolve all wave modes. In the *pseudospectral* method, the nonlinear terms appearing in Eqs. (1)-(3) (or in any other of the PDEs considered) are computed in physical space, and then transformed into spectral space using the multidimensional Fourier transform, in order to obviate the need to compute the convolution integrals explicitly, which is expensive. Since the pressure is a Lagrange multiplier, its action is taken by projecting the nonlinear term in spectral space onto a divergence-free space, so that the velocity update will satisfy Eq. 3. If not for the physical space computation of nonlinear terms, the method, as is done in pure spectral codes, would solve the PDEs entirely in spectral space.

The global physical domain may be represented schematically as shown in Fig. 1 (left). The domain is decomposed in the vertical direction (a so-called 1D or *slab* decomposition) in such a way that the vertical planes are evenly distributed to all MPI tasks (the slabs will be further decomposed into smaller domains using OpenMP, as described below). A relatively common alternative to this approach is to use a 2D “pencil” decomposition (Yeung et al., 2005; Chatterjee et al., 2018), whose performance implications were considered in **M11**. If  $P$  is the number of MPI tasks, there are  $M = N_z/P$  planes of the global domain assigned as work to each task, and from the figure, it is clear that each task “owns” a slab of size  $N_x \times N_y \times M$  points. The forward transform (for the moment, only considering MPI parallelization) consists of three main steps:

1. A local 2D transform is carried out on the real physical data in each plane (lightly shaded in the figure) of the local slab, over the coordinates indicated by the arrows in Fig. 1 (left), which produces a partial (complex) transform that is *z-incomplete* because of the domain decomposition.

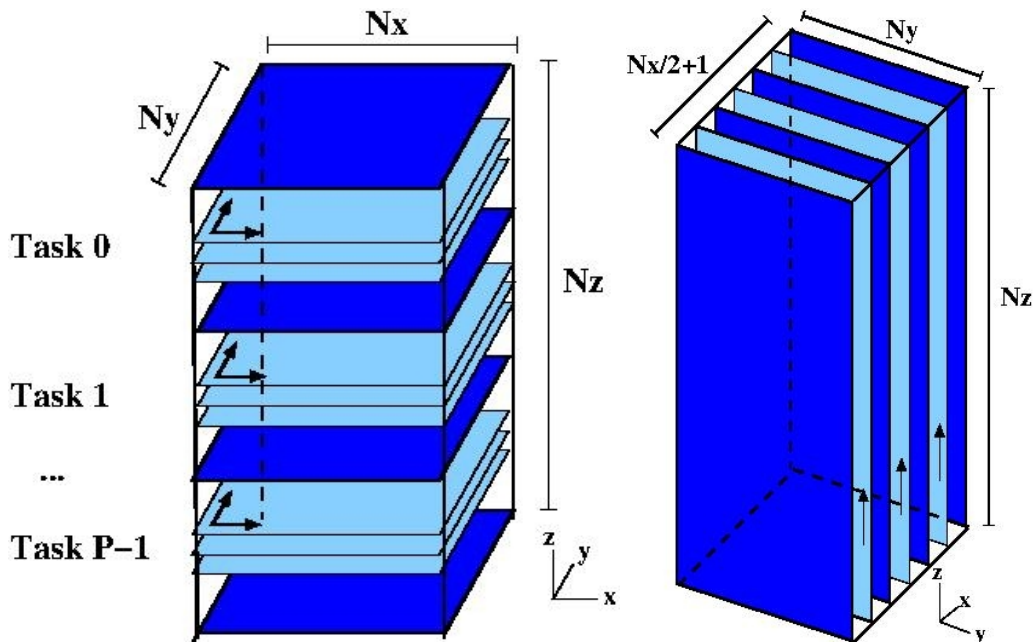


Figure 1: Schematic of the global grid, and its 1D or slab-based domain decomposition used for the global Fourier transform. *Left* shows the real data block in physical space, together with the decomposition of the block among MPI tasks, where the dark shaded planes indicate MPI task boundary. This decomposition highlights the  $z$ -incompleteness (and  $x$ - and  $y$ -completeness) of the physical space data. The first step of the global transform is indicated by the arrows and represent a local 2D transform in each plane of the slab owned by the task, indicated by the lightly shaded planes. On the *right* the original data block has been transposed in a second global transform step, so that the partially transformed data on the left is now  $z$ - and  $y$ -complete (and  $x$ -incomplete), in order that the final step in the global transform may be done: a final 1D transform done in the direction of the arrow for the data in each of the complex (shaded) planes.

2. Next, a global transpose (Fig. 1, right) of the partially transformed data block is made so that the data becomes  $z$ - and  $y$ -complete (and, hence,  $x$ -incomplete).
3. Finally, a local 1D transform is performed in the now complete  $z$ -direction for each plane of the data in the partially transformed slab (indicated by an arrow on the lightly shaded planes in Fig. 1(b)), producing a fully transformed data block.

Note that the total number of data points in Fig. 1 (left) is now  $(N_x/2 + 1) \times N_y \times N_z$ , and reflects the fact that the data is now complex, and that the transform satisfies the relation  $\hat{\phi}(\mathbf{k}) = -\hat{\phi}(-\mathbf{k})$  (assuming the data in physical space is real). However, the *total* amount of complex (real and imaginary) data is still the same as in the original data block. The reverse transform essentially reverses these steps to produce a real physical space field. On the CPU the local transforms are computed using the Fast Fourier Transform (FFT) in the open source FFTW package (Frigo and Johnson, 1998, 2005).

The global transpose in the second step requires that all MPI tasks communicate a portion of their data to all other tasks, in an MPI all-to-all. This is handled using a non-blocking scheme detailed in (Gómez et al., 2005; Mininni et al., 2011), so we do not describe it further here, except to state this MPI communication is the only communication involved in the solution of the PDEs, and that it usually represents a large fraction of the global transform time, as seen below. In addition to the communication, the data local to each task must also be transposed, which can be identified as a separate computational cost. Thus, the three steps involved in computing the global FFT transform yield in turn three distinct operations whose costs (times) will be considered further below: (1) the local FFT (i.e., computation of the 2D and 1D FFTs), (2) communication (to do the global transpose), and (3) the local transpose of data.

Our previous work in **M11** demonstrated how OpenMP directives enable loop-level thread parallelization of the algorithm described above to compute parallel forward transforms, its implementation in the MPI-parallelized GHOST

code, and provided a detailed examination of single NUMA node performance as well as a discussion of scaling to large core counts. This thread parallelization, on top of the MPI parallelization, results in operations performed by each thread over a smaller portion of the slab that belongs to each MPI task, and thus can be equivalent (depending on the number of MPI tasks and threads) to a pencil decomposition, in which the MPI tasks operate over slabs, and the threads over pencils in each slab. While the motivation in **M11** was mainly to show the overall efficacy of this hybrid MPI-OpenMP parallelization scheme, we also described the specific directives for thread parallelization and the cache-blocking procedure used for the local transpose step. Because of the centrality of the transform, we investigate here the effect of placing as much as possible of the multidimensional Fourier transform on GPUs using CUDA, while leaving other operations done by the CFD code in the CPUs. Thus, the method we present has three layers of parallelization: MPI and OpenMP for operations done in the CPUs, and CUDA for the operations that will we moved to the GPUs.

In order to estimate the benefit of a potential GPU port of the transform, we consider timings of the basic transform operations in typical simulations at various resolutions. In Table 1 are presented fractional timing results of runs solving Eqs. (1)-(3) on uniform isotropic 3D grids of size  $N_x = N_y = N_z = N$  for  $N = 128, 256, 512,$  and  $1024$ . These runs were made on the NCAR-Wyoming Cheyenne supercomputer using 4 MPI tasks per node without threading. Each core is an Intel Xeon E5-2697 v4 (Broadwell), and the interconnect topology is an enhanced hypercube. No attempts were made to optimize MPI communication via task placement or changes to the default MPI environment. As with all subsequent timing results, the code runs in “benchmark” mode in which all computations are performed in solving the PDEs—thus, both forward and backward transforms are done—but with no intermediate I/O for  $O(10)$  time steps, and the overall time as well as the operation (component) times are averaged over this number of time steps. The table provides the fraction of total average runtime spent on each of the transform operations identified above.

The sum of the fractional times shows that the cumulative time fraction of the distributed transform (counting FFTs, communication, and transpose) is high, and reasonably constant at about 90%, which justifies our focus on the distributed transform in isolation from the remaining computations. Indeed, the last column in Table 1 shows the maximum speed-up that could be achieved if the time to do FFTs and transposition is reduced to zero (leaving communication time the same). In terms of the component times (where  $t_R^{\text{CPU}}$  represents costs not included in the transform), we can estimate this maximum possible speed-up *assuming no additional costs* by offloading to an accelerator as:

$$\begin{aligned} S &\approx (t_{\text{Comm}}^{\text{CPU}} + t_{\text{FFT}}^{\text{CPU}} + t_{\text{Transp}}^{\text{CPU}} + t_{\text{R}}^{\text{CPU}}) / (t_{\text{Comm}}^{\text{CPU}} + t_{\text{R}}^{\text{CPU}}) \\ &= 1 + (t_{\text{FFT}}^{\text{CPU}} + t_{\text{Transp}}^{\text{CPU}}) / (t_{\text{Comm}}^{\text{CPU}} + t_{\text{R}}^{\text{CPU}}), \end{aligned}$$

where the denominator approximates the aggregate runtime by using acceleration on the distributed transform, assuming  $t_{\text{FFT}}^{\text{GPU}}$  and  $t_{\text{Transp}}^{\text{GPU}}$  both go to 0, and that  $t_{\text{Comm}}^{\text{CPU}}$  does not change by simply adding the accelerators. Here,  $t_X^{\text{CPU}}$  indicates the time to compute the operation X when using CPUs only, where X can be communication (Comm), local FFTs (FFT), or local transpose (Transp). Since the aggregate time fraction of the transform component is so high, we can neglect  $t_{\text{R}}^{\text{CPU}}$ . The final column in Table 1 gives this potential speed-up for each resolution.

This estimate indicates that speed-up is strongly connected to performance of the local FFT and transform relative to the communication time. While the potential speed-ups in the table may look impressive, any optimization that serves to reduce the time for the FFT and transpose on the CPU relative to the communication time will also reduce the speed-up. An obvious optimization on the CPU is threading (which is already implemented in the code, as discussed above), but we will see in Sec. 4 that the realized speed-ups when using GPUs are still superior to the purely CPU-based code even when multithreading is enabled.

### 3. CUDA implementation

The basic CUDA implementation of the distributed transform involves interfacing directly or indirectly with CUDA code and primarily with the CUDA runtime and cuFFT libraries. We describe in the following subsections how this is accomplished in GHOST.

#### 3.1. Preliminaries

As mentioned in Sec. 2, our goal for the GPU implementation of the distributed transform is to place as much work on the device as possible for as long as possible, in order to reduce the number of transfers. Of the three

Table 1: Fraction of total runtime for each of the main operations involved in the distributed transform: FFTs ( $f_{\text{FFT}}$ ), transpose ( $f_{\text{Transp}}$ ), and communications ( $f_{\text{Comm}}$ ), for runs done with different linear resolutions  $N$  and number of cores  $N_c$ . The remainder of the time in each run is spent on other computations. The last column gives the maximum speed-up possible if the cost for the local FFTs and transposes are driven to zero.

$N$	$N_c$	$f_{\text{FFT}}$	$f_{\text{Transp}}$	$f_{\text{Comm}}$	Max Speed-Up
128	16	0.68	0.08	0.13	7
256	32	0.62	0.1	0.17	5
512	64	0.61	0.09	0.21	4
1024	128	0.62	0.08	0.22	4

operations involved in the transform, the communication alone will be explicitly handled on the CPU, although future work will examine the ability of NVIDIA GPUDirect™ to at least reduce latency in transferring data directly to and from the network. The other two operations, the local transpose and local FFTs are handled with interfaces to CUDA kernels, the former to our own CUDA transpose kernel and the latter to the cuFFT library. GHOST is mainly a Fortran 90/95/2003 code so for interfacing directly or via C wrappers with CUDA we rely heavily on ISO C bindings. All calls to C or CUDA from the GHOST code occur by way of ISO C bindings which standardize the Fortran-to-C datatypes and also prevents us from having to maintain C function wrappers that accommodate compiler-specific name-mangling. A single ISO C binding interface is written for each routine called in the cuFFT, the CUDA runtime library, or made to a C function that we have written to, say, launch a CUDA kernel. An example of a binding is given in the listing below, in which the CUDA runtime function name is specified in the **bind** clause, and the function name called from Fortran is taken in this example to be the same:

```
! *****
! cudaHostAlloc
! *****
INTEGER(C_INT) function cudaHostAlloc(buffer, isize, flags) &
    bind(C, name="cudaHostAlloc")
    USE, INTRINSIC :: iso_c_binding
    IMPLICIT NONE
    TYPE(C_PTR) :: buffer
    INTEGER(C_SIZE_T), value :: isize
    INTEGER(C_INT), value :: flags
END FUNCTION cudaHostAlloc
```

Many of the CUDA runtime or cuFFT library calls require parameters, or provide return values that may be examined, and are standardized. We have classified these as directives (such as cuFFT\_R2C, that tells cuFFT the direction in which to compute the transform on the GPU), return codes both for cuFFT and the CUDA runtime library, and finally, device properties. The cuFFT directives and return codes are taken from the library header files, and encoded in a Fortran 90 module as parameters. Similarly, the CUDA runtime return codes are translated from the CUDA headers to a Fortran 'enum' type with C binding:

```
ENUM, BIND(C)
    ENUMERATOR ::
        cudaSuccess =0 , &
        cudaErrorMissingConfiguration =1 , &
        cudaErrorMemoryAllocation =2 , &
        cudaErrorInitializationError =3 , &
        cudaErrorLaunchFailure =4 , &
        cudaErrorPriorLaunchFailure =5 , &
        ...
END ENUM
```

Finally, the CUDA device properties structure is also taken from the CUDA header files and made interoperable with Fortran by encapsulating within a Fortran structure with C binding. This type may therefore be passed as a datatype to CUDA device property runtime calls. This structure takes the form:

```
TYPE, BIND(C) :: cudaDevicePropG
    INTEGER (C_INT) :: canMapHostMemory
```

Listing 1: Partial listing of the GFFTPLAN\_DATA distributed plan data type. This structure is contained within the GHOST transform module. It contains the declarations for the Fortran host pointers **carr**, **ccarr**, **rarr**, the device pointers used in cuFFT calls, **cu\_dd**, **cu\_ccd**, **cu\_rd**, and the host **C\_PTR** blocks, **pcarr**, **pccarr**, and **prarr** for passing host data to CUDA runtime functions. The size variables **sz\*** give the byte size of each host (and device) array. CUDA stream pointers and local data sizes are provided in **pstream** and **str\_\***, respectively (*cf.*, Sec. 3.3). Handles for the local cuFFT plans for real-to-complex (**icuplanrc**) and complex-to-real (**icuplanr**) transforms are also contained within this larger encapsulating plan.

```

USE iso_c_binding
TYPE GFFTPLAN_DATA
  COMPLEX(KIND=GP),POINTER,DIMENSION(:,:,:) :: carr,ccarr
  REAL(KIND=GP),POINTER,DIMENSION(:,:,:) :: rarr
  TYPE(C_PTR) :: pcarr,pccarr,prarr
  TYPE(C_PTR) :: cu_cd,cu_ccd,cu_rd
  TYPE(C_PTR),DIMENSION(nstreams) :: pstmtream
  INTEGER(C_SIZE_T) :: szcd,szccd,szrd
  INTEGER(C_SIZE_T),DIMENSION(nstreams) :: str_szcd,str_szccd,str_szrd
  INTEGER(C_SIZE_T),DIMENSION(nstreams) :: icuplanrc,icuplanr
  ...
END TYPE GFFTPLAN_DATA

  ...

  INTEGER (C_INT) :: clockRate
  INTEGER (C_INT) :: computeMode
  INTEGER (C_INT) :: deviceOverlap
  INTEGER (C_INT) :: integrated
  INTEGER (C_INT) :: kernelExecTimeoutEnabled
  ...
END TYPE cudaDevicePropG
  iret = cudaHostAlloc ( plan%pccarr_, plan%szccd_, cudaHostAllocPortable )

```

### 3.2. Memory management

The distributed transform in GHOST is a Fortran 90 module that handles everything from set up to cleanup. The set up works in the same vein as FFTW (Frigo and Johnson, 1998, 2005), by creating a 'plan' for the distributed transform. The plan contains all data required for the local FFTs, transposes and communication, and it also creates and maintains the device pointers and other data required to perform local operations on the GPU. Though in operation there are separate plans for each of the forward and backward distributed transforms, the data allocated to each plan is shared. It is also the responsibility of the GHOST plan to create the cuFFT plans that are used to carry out the local CUDA FFT transforms.

Non-device local data that are passed to CUDA runtime functions, *e.g.*, for copying to and from device memory, are declared within the module as of **TYPE(C\_PTR)**. An example of such declarations is provided in Listing Listing 1. The plan establishes the sizes required for each of these quantities, and these are determined by the size and datatype of the input data. There is a **TYPE(C\_PTR)** declaration for each type of data the cuFFTs need, but the same data is used for the forward and backward transforms. They are, in all respects, standard C pointers. Each of these **TYPE(C\_PTR)** variables is allocated on the CPU host in the creation step for a distributed plan with a call in Fortran like

```

  iret = cudaHostAlloc(plan%pcarr , plan%szcd , cudaHostAllocPortable)
  iret = cudaHostAlloc(plan%ppcarr , plan%szccd , cudaHostAllocPortable)
  iret = cudaHostAlloc(plan%prarr , plan%szrd , cudaHostAllocPortable)

```

using the **cudaHostAlloc** CUDA runtime function. This function allocates page-locked (*pinned*) memory that can be accessed directly by the GPU at higher bandwidths than, say, with **malloc**. In Sec. 3.3, we will see that this is also required for asynchronous data transfer. In all cases, the **cudaHostAllocPortable** flag is used to specify that the memory is pinned in all CUDA contexts. Note in this call that the **C\_PTR** type, and the data size are contained within the distributed plan (see also Listing 1). Each **cudaHostAlloc** is paired with a call

```

  iret = cudaFreeHost (plan%pccarr)

```

in the clean up method of the plan, in order to free the host memory properly.

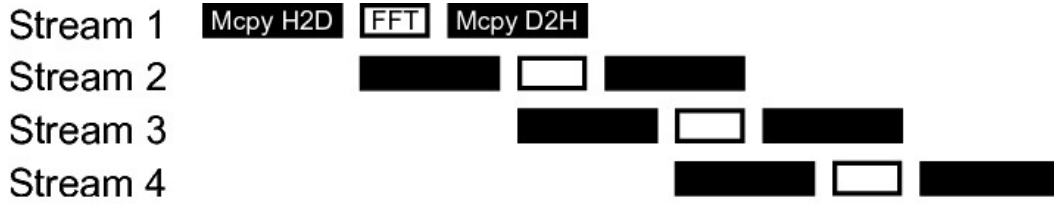


Figure 2: Schematic of CUDA stream use to overlap data transfer from the host to the device (H2D) with cuFFT computation. Each stream operates on only a section of the data block. The data is transferred asynchronously, and the computation starts on a stream as soon as the data transfer is complete. Black “Mcpy H2D” (“D2H”) boxes indicate copies of the data from the host to the device (or *vice versa*), while white “FFT” boxes correspond to the computation of the FFTs on the data available in that stream.

Once this pinned host memory is allocated, the “traditional” Fortran arrays can be associated with it for use in purely host-based operations, like MPI communication, host copies, etc. The plan therefore declares an associated Fortran *pointer* of the required signature (type and rank). This Fortran pointer is associated with the corresponding **C\_PTR** block using the following ISO C binding runtime call:

```
CALL c_f_pointer(plan%pcarr ,plan%carr , (/Nx/2+1,Ny,kend-ksta+1/))
CALL c_f_pointer(plan%pccarr ,plan%ccarr , (/Nz,Ny,iend-ista+1/))
CALL c_f_pointer(plan%prarr ,plan%rarr , (/Nx,Ny,kend-ksta+1/))
```

Note that, *ksta* (*kend*), and *ista* (*iend*), refer to the bounding indices of the global grid that define the work region of each MPI task, as described in Sec. 2: The *k*-bounds are required due to the *z*-incompleteness of the real and partially transformed data (**rarr** and **carr**), and the *i*-bounds are required because of the *x*-incompleteness of the the full complex transform (**ccarr**) as shown in Fig. 1 (left) and Fig. 1 (right), respectively. Thus, while the manifestly Fortran arrays are *not* the central, allocated quantities used in the distributed transform method on the host, due to the interfaces with cuFFT and CUDA runtime, the **C\_PTR** host blocks are.

Lastly, the device pointers contained within the plan are created:

```
iret = cudaMalloc(plan%cu_cd , plan%szcd )
iret = cudaMalloc(plan%cu_ccd , plan%szccd )
iret = cudaMalloc(plan%cu_rd , plan%szrd )
```

These calls, and the scope of these device pointers within the transform module, allow for the persistence of the pointers until the the plan’s clean up method is called.

### 3.3. CUDA streams for overlapping device data transfer and computation

CUDA streams are used in an attempt to overlap the data transfer to the device for local cuFFT device computations (Sanders and Kandrot, 2011). The basic procedure is illustrated in Fig. 2, and involves three distributed transform *plan execution* steps: (1) copying the data for each stream to the device asynchronously using **cudaMemcpyAsync**, (2) performing the local FFT on the device using the appropriate *streamed* cuFFT method for the local FFT being computed, and (3) having each stream copy the data back to the host again using **cudaMemcpyAsync**. The local cuFFT task is completed by calling the **cudaStreamSynchronize**, after which we are guaranteed that the computation has completed. Each of these steps is done in a “batch” process for the entire set of streams by the main thread. We emphasize that the batch processing by the main thread highlights the fact that a single GPU is bound to a single MPI task.

As mentioned in Sec. 3.2, the host and device storage for each of these operations, as well as the data sizes, are computed in the GHOST plan creation routine. The CUDA streams are also created there using **cudaStreamCreate**, and they are destroyed using a call to **cudaStreamDestroy** in the GHOST plan clean up method. If the local transpose operation (*cf.*, Sec. 2) is performed on the device, as it is for the results presented below, execution step (3) must be postponed until after the transpose is complete.

In each batch call in execution step (2), each stream calls the appropriate cuFFT function with a cuFFT plan created for that stream. These plans are created in the GHOST plan creation method; the local plan handles are carried in the GFFTPLAN\_DATA in Listing 1, where **icuplanrc** are the plan handles for real-to-complex transforms,



Listing 2: Partial code listing of the GHOST plan creation code showing the creation of the streams and the local stream cuFFT plans for 2D real-to-complex cuFFTs.

```

DO i = 1, nstreams
    irect = cudaStreamCreate( pstream( i ) )
ENDDO
nrank= 2
DO i = 1, nstreams
    CALL range( ista , iend , nstreams , i-1, first , last )
    issta ( i ) = first
    issnd ( i ) = last
    CALL range( ksta , kend , nstreams , i-1, first , last )
    kssta ( i ) = first
    kssnd ( i ) = last
    plan%str_szccd( i ) = max( 2* Nz      *Ny*( issnd( i )- issta( i )+1) &
                               *GFLOATBYTESZ, GFLOATBYTESZ )
    plan%str_szcd ( i ) = max( 2*(Nx/2+1)*Ny*( kssnd( i )- kssta( i )+1) &
                               *GFLOATBYTESZ, GFLOATBYTESZ )
    plan%str_szrd ( i ) = max(   Nx      *Ny*( kssnd( i )- kssta( i )+1) &
                               *GFLOATBYTESZ, GFLOATBYTESZ )

    na      ( 2 ) = Nx      ; na      ( 1 ) = Ny ;
    pinembed( 2 ) = Nx      ; pinembed( 1 ) = Ny*( kssnd( i )- kssta( i )+1);
    ponembed( 2 ) = Nx/2+1 ; ponembed( 1 ) = Ny*( kssnd( i )- kssta( i )+1);
    istr     = 1          ; idist    = Nx*Ny   ;
    ostr     = 1          ; odist    = Ny*(Nx/2+1) ;
    irect = cufftPlanMany( plan%icuplanrc( i ), nrank, na, pinembed, istr, idist, &
                          ponembed, ostr, odist, CUFFT_R2C, kssnd( i )- kssta( i )+1);
ENDDO

```

and **icuplanrc** are those for complex-to-real transforms. Each of these local stream plans uses the cuFFT “advanced data layout” for batch processing of FFTs. These local plans specify the data stride between successive input and output elements, and the number of input and output elements for the FFT. Offsets for the the input and output data in the **cudaMemcpyAsync** in steps (1) and (3) above may also be computed in the GHOST plan creation step, and carried in the plan data for use on demand. These same offsets can be used in the calls to the cuFFT routines in execution step (2) to specify the starting location of the input and output data for a stream (see Listing 3). Note that the actual data passed to the **cudaMemcpyAsync** call and to the cuFFT routines are just the host **C\_PTR** blocks and the device pointers discussed in Sec. 3.2 and stored in **GFFTPLAN\_DATA**. Sample code for creating the real-to-complex plans is provided in Listing 2. The **range** routine in this listing computes for each stream indices that are comparable to the quantities *ksta* (*kend*), and *ista* (*iend*) denoting the bounds of an MPI task’s subdomain in Sec. 3.2, but in this case it returns the beginning and end of data chunks in each stream. The value of **GFLOATBYTESZ** is a constant parameter that specifies the byte size of the configurable GHOST floating type.

A code sample of the three transform execution steps is provided in Listing 3 for (most of) the forward distributed transform. This code shows explicitly the “batching” of the three execution steps using CUDA streams, as well as the use of the host and device data previously discussed when interfacing with the CUDA runtime and cuFFT calls. Code for the computation of the local data transpose and for the final 1D batch cuFFT of the now *x*-complete data is omitted, but indicated.

Additional comments about our GPU implementation are warranted. In general, a maximum number of streams allowed is set at build time. But not all GPUs support overlapping data transfer with computation as we have outlined. One should use **cudaGetDeviceProperties** to check the **deviceOverlap** field of the **cudaDeviceProp** structure, in order to determine if overlapping data transfer with computation is supported on a given device. If not, **nstreams** should be set to 1 in Listing 2. Because a single MPI task is bound to a single GPU, we cannot at this time use the multiple GPU cuFFT transforms that are available available in cuFFT 8 (NVIDIA, 2018b). Finally, it is worth pointing out that even when CUDA is used in the distributed transform, the code not operating on the device may still be threaded as discussed in **M11**. Given that the implementation binds an MPI task to a single device, the extra threading is able to exploit effectively multicore nodes that have significantly fewer GPUs than compute elements. Thus, and as previously mentioned, the code can utilize three levels of parallelization: a coarse (MPI) level, a finer-

Listing 3: Partial code listing the forward GHOST transform plan execution. The three execution steps are seen clearly. The byte offsets for the input and output data are given explicitly here. Note the association of the cuFFT plans with their corresponding streams. This must be done prior to any batch cuFFT calls using a new plan so that the streamed cuFFT API can be used. The `cudaMemCpyAsyncOffDev2Host` is simply an ISO C-bound wrapper to the `cudaMemcpyAsync` that applies the offsets locating the appropriate input and output data for that batch call.

```

DO i = 1,nstreams ! Associate cuFFT plans with streams
  iret = cufftSetStream( plan%icuplanr(i), pstream(i));
END DO
plan%rarr = real_input_data ! Copy real input data to host pointer
DO i = 1,nstreams ! Batch copy of input data to device
  byteoffset1 = plan%Nx*plan%Ny*(kssta(i)-ksta)*GFLOATBYTESZ
  byteoffset2 = plan%Nx*plan%Ny*(kssta(i)-ksta)*GFLOATBYTESZ
  iret = cudaMemcpyAsyncOffHost2Dev( plan%cu_rd, & ! Dev
                                     byteoffset1, & ! OFFSET Dev
                                     plan%prarr, & ! Host
                                     byteoffset2, & ! OFFSET Host
                                     plan%str_szrd(i), pstream(i) )
END DO
DO i = 1,nstreams ! Batch 2D cuFFT
  byteoffset1 = plan%Nx*plan%Ny*(kssta(i)-ksta)*GFLOATBYTESZ
  byteoffset2 = 2*(plan%Nx/2+1)*plan%Ny*(kssta(i)-ksta)*GFLOATBYTESZ
  iret = cufftExecOffR2C( plan%icuplanr(i), plan%cu_rd, & ! Dev
                          byteoffset1, & ! OFFSET Dev
                          plan%cu_cd, & ! Dev
                          byteoffset2) ! OFFSET Host
END DO
DO i = 1,nstreams ! Batch copy from device to host
  byteoffset1 = 2*(plan%Nx/2+1)*plan%Ny*(kssta(i)-ksta)*GFLOATBYTESZ
  byteoffset2 = 2*(plan%Nx/2+1)*plan%Ny*(kssta(i)-ksta)*GFLOATBYTESZ
  iret = cudaMemcpyAsyncOffDev2Host( plan%pcarr, & ! Host
                                     byteoffset1, & ! OFFSET Host
                                     plan%cu_cd, & ! Dev
                                     byteoffset2, & ! OFFSET Dev
                                     plan%str_szcd(i), pstream(i) )
END DO
DO i = 1,nstreams ! Batch synchronization
  iret = cudaStreamSynchronize(pstream(i))
END DO
! <Do local transpose step>
! <Do final batch local ID transform in x-complete direction>

```

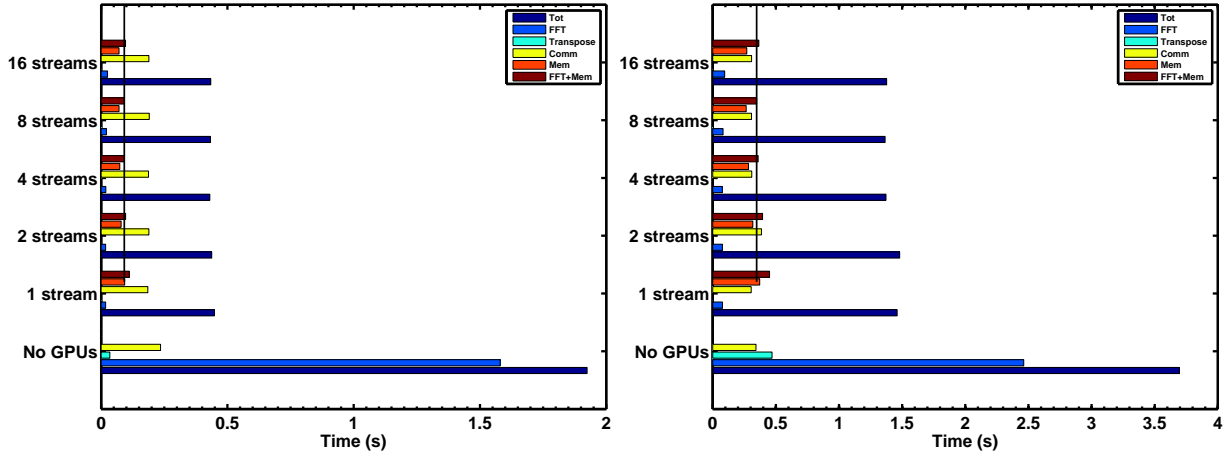


Figure 3: Total time (Tot) and operation times for GPU runs (time to compute FFTs, transpose, MPI communication, memory copy from and to the GPU, and FFTs plus copies) with varying number of CUDA streams. *Left*: In the system with NVLink, and *right*: in the PCIe system. The minimum transfer time in both cases is seen for  $\mathbf{nstreams} = 8$ , and its time  $t_{\text{FFT}} + t_{\text{Mem}}$  is indicated by the dark vertical line (compare the increase in this time for  $\mathbf{nstreams} = 1$ ). In the bottom of each figure, the total and component times (excluding device transfer time) are provided for a corresponding CPU-only run using the same number of MPI tasks and threads per task.

grain CPU threading level (OpenMP), and a fine grain (GPU) level. All three will be in used in Sec. 4.

#### 4. Results: scaling and performance

A series of tests have been performed to evaluate the implementation discussed in Sec. 3. Most of these tests have been conducted on Oak Ridge Leadership Computing Facility’s SummitDev system, which contains 54 nodes each with 2 IBM Power8 chips (10 cores each) and 4 NVIDIA Tesla P100 GPUs. The nodes utilize a full fat-tree network via EDR InfiniBand; the GPUs are connected by NVLink 1.0 at 80GB/s, and we use CUDA 9. For all tests using this system, we restrict ourselves to 16 of the 20 CPU cores on each node. Using runtime directives, the MPI tasks are placed symmetrically across the sockets, and threads from each socket are bound to their respective tasks; the GPUs are selected to optimize data transfer. When stated, for comparison purposes, we have also run on the NCAR-Wyoming Caldera analysis and visualization cluster. This system contains 30 nodes, each containing 2 8-core Intel Xeon E5-2670 (Sandy Bridge) CPUs, and 16 of which contain two NVIDIA Tesla K20Xm GPUs using PCIe Gen2 bus, and only CUDA 8 is available.

The test procedure is the same as described in Sec. 2, and the resulting timing output contains the total average runtime per time step ( $t_{\text{Total}}$ ), and the component operation times for the local FFTs ( $t_{\text{FFT}}$ ), for the the MPI communication ( $t_{\text{Comm}}$ ), and for the transpose time ( $t_{\text{Transp}}$ ). The additional data transfer time ( $t_{\text{Mem}}$ , to and from the GPUs) now also appears. These times are measured by the main thread using primarily the MPI.WTIME function, and, on the GPU, the timers wrap the entire kernel launch and execution. We compared the results of these times with Fortran, OpenMP, and CUDA timers, to verify consistency. In addition to the solver for Eqs. (1)-(3), we now also examine briefly the other solvers in Sec. 2, since we want to evaluate the performance when different sets of PDEs are used (requiring different numbers of distributed transforms). As with timings of Eqs. (1)-(3) presented in Sec. 2, we examine aggregate timings that reflect complete solutions to the equations being considered, not just of the transform kernels. Thus, component times are accumulated over both the forward and backward transforms that occur in a timestep before averaging over the number of timesteps integrated.

##### 4.1. Variation with $\mathbf{nstreams}$

We examine first the performance of the CUDA streams for overlapping communication and computation. The pure HD equations are used here (so the temperature evolution equation Eq. 2 is omitted, as is the temperature term in

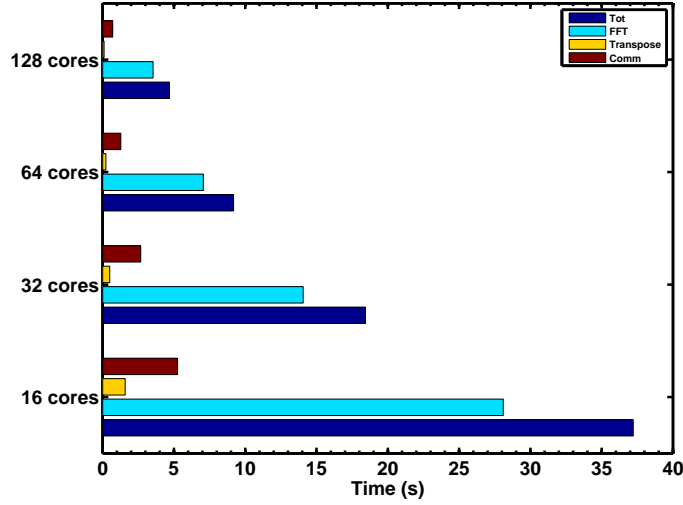


Figure 4: Process timers (total time and operation times) for CPU-only Boussinesq runs on an anisotropic grid using various core counts, with  $n_{\text{thd}} = 8$  (thus, the number of MPI tasks is equal to the number of cores used divided by  $n_{\text{thd}}$ ). Timings correspond to the system with NVLink. Note the nearly ideal scaling of each of the timers with core-count.

Eq. 1). Therefore, there are seven less distributed transforms required compared when compared to the full system of Eqs. (1)-(3) (as the HD system has one less nonlinear term when compared with the Boussinesq system). The grid is taken to be isotropic with  $256^3$  points. Sixteen cores and 2 GPUs of one SummitDev node are used; since each GPU is bound to a single MPI task, this implies that 2 MPI tasks each with 8 threads are used. Fig. 3 (left) shows the timings as the number of CUDA streams is varied in this system, at the bottom the times are compared to a CPU-only run. The first thing seen in the figure is that there is a good speed-up over the CPU-only case, about a factor of 4.4, achieved with the best GPU time. As expected, the FFT and local transforms times have been reduced significantly, by factors of 85 and 1300 respectively, making them nearly negligible in the GPU runs. Unexpectedly, the communication time for the identical run without GPUs is somewhat longer than for the GPU runs, and this behavior is persistent for this problem.

Since both the local FFTs and the device transfers add up to the total time to compute FFTs in the GPUs, we must add the two measured times in order to determine the optimal number of streams. The  $n_{\text{streams}} = 4$  and 8 runs yield nearly the same aggregated time  $t_{\text{FFT}} + t_{\text{Mem}}$ , but  $n_{\text{streams}} = 8$  gives a slightly better result, so we adopt this as the optimal number of streams for subsequent tests. The speed-up,  $S_{\text{FFT+Mem}}$ , over the time to move data to and from the GPU and to compute the FFTs, for  $n_{\text{streams}} = 8$  over that for  $n_{\text{streams}} = 1$ , is 21%. Testing on the PCIe system for comparison (see Fig. 3, right) we also find that  $n_{\text{streams}} = 8$  gives the best times, but that  $S_{\text{FFT+Mem}} = 30\%$ , a larger effect due to importance of using stream optimization in the slower PCIe port. As expected, the PCIe transfer times are uniformly slower than for NVLink (see Fig. 3). Because of this, the improvement when using multiple streams on the total runtime of the CFD code (when compared with the case using GPUs with 1 stream) is about 3% on the NVLink system, versus 5% on the PCIe system with the optimized streamed transforms. Similar results were obtained when varying  $n_{\text{streams}}$  for anisotropic grids with  $N_x \neq N_y \neq N_z$ , and for other PDEs.

Heuristically, the aggregate speed-up,  $S_{\text{agg}}$ , afforded by the (streamed) GPU transforms over the CPU-only version on this system may be computed by setting the GPU times  $t_{\text{FFT}}^{\text{GPU}}$  and  $t_{\text{Transp}}^{\text{GPU}}$  to zero (see Fig. 3), yielding

$$S_{\text{agg}} = \frac{t_{\text{Total}}^{\text{CPU}}}{t_{\text{Total}}^{\text{GPU}}} \quad (9)$$

$$\approx \frac{t_{\text{Total}}^{\text{CPU}}}{t_{\text{Comm}}^{\text{CPU}} + t_{\text{R}}^{\text{CPU}} + t_{\text{Mem}}}, \quad (10)$$

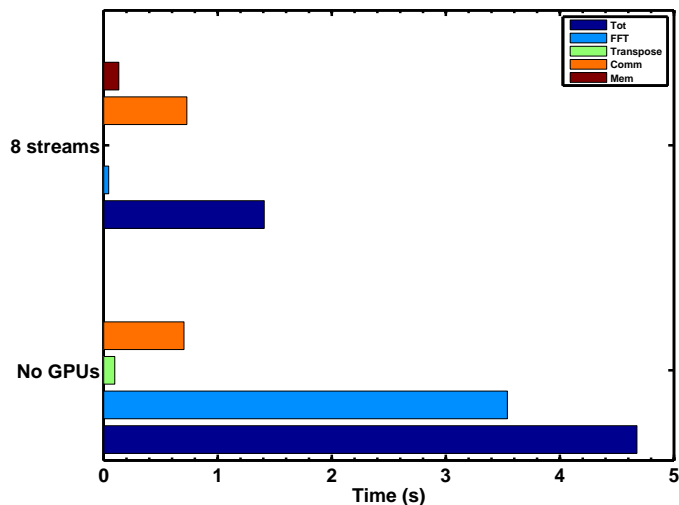


Figure 5: Comparison between the MPI-OpenMP CPU-only code, and the multi-level (MPI-OpenMP-CUDA) parallel timings ( $nstreams = 8$ ) for a Boussinesq run on a grid of  $1024 \times 1024 \times 256$  points in the system with NVLink. A total of 32 cores (2 nodes) were used in both cases (in the case with GPUs, this corresponds to 8 GPUs). The overall speed-up of the GPU- to the CPU-based run is 3.3.

where  $t_R^{CPU} = t_{Total}^{CPU} - t_{Comm}^{CPU} - t_{FFT}^{CPU}$  is the remainder of the time spent on the CPU that is unrelated to distributed transform operations. For these tests,  $t_R^{CPU} \approx 0.1$ . Plugging in the values  $t_{Comm}^{CPU} \approx 0.2$ ,  $t_R^{CPU} \approx 0.1$ , and  $t_{Mem} \approx 0.1$  for this stream test yields  $S_{agg} \approx 4.8$ , which is very close to the observed speed-up. As expected, the speed-up results from the gains in the FFT computed in the GPUs, minus the cost of moving the data to the device (which is reduced by overlapping memory copies and computation using multiple streams). From this value we also see that the speed-ups obtained are close to the maximum we can achieve (given the fraction of computations that were moved to the GPUs, see also Table 1), and we thus now consider the scaling of the method with increasing number of MPI tasks and GPUs.

#### 4.2. Baseline CPU-only runs on anisotropic grid

As a reference, we consider first a set of CPU-only runs solving the Boussinesq equations, Eqs. (1)-(3), on an anisotropic grid (Sojovolosky et al., 2018), using the system with NVLink. In Fig. 4 we present a series of runs with the number of threads  $n_{thd} = 4$  for each MPI task, using various core counts (and, hence, number of nodes). The anisotropic domain consists of  $1024 \times 1024 \times 256$  grid points, and the figure shows a histogram of strong scaling of each timer with core count. Indeed, the plot indicates that each operation scales well on this system, and that the fractional time for the distributed transform is very similar to those in Table 1. The average parallel efficiency  $\varepsilon = N_c T / (N_{c,0} T_0)$ , with respect to the reference aggregate time  $T_0$  at the smallest core count  $N_{c,0}$ , is about 99% for this problem.

#### 4.3. Speed-Up and scaling with full parallelization

We can now consider the speed-up and scaling of the code in the context of the Boussinesq equations with the anisotropic grid of  $1024 \times 1024 \times 256$  points, using full MPI, OpenMP and GPU parallelization. For all runs in this section, we use the same configuration of MPI tasks, GPUs and threads on each node as in Sec. 4.1, varying the number of nodes when required to increase the number of MPI tasks (and therefore, of GPUs). In Fig. 5 we first present operation times for both GPU and CPU runs on the fiducial NVLink test system using a fixed number of 32 cores (2 nodes). We see an aggregate speed-up of the GPU case over the CPU case of 3.3. Like in Sec. 4.1, we observe that the FFT and local transpose times have been reduced significantly by factors of 80 and 200, respectively.

In Fig. 6 the scaling is presented of the same  $1024 \times 1024 \times 256$  runs as in Fig. 5, but to larger core and GPU counts. As with the CPU-only results in Fig. 4, the component times and total runtimes appear to scale well with GPU count

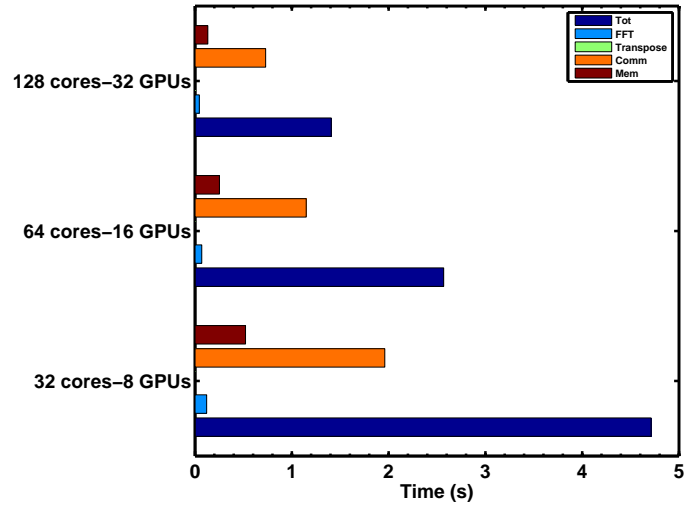


Figure 6: Strong total and per component scaling for the problem as in Fig. 5, presenting all the times measured in GPU-based runs varying the number of MPI tasks and of GPUs, in the system with NVLink. These can also be compared with the associated CPU-only run in Fig. 5.

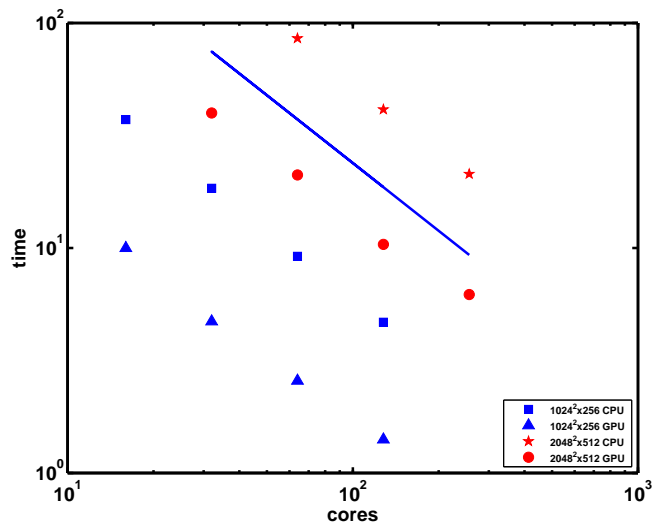


Figure 7: Traditional strong scaling plot for anisotropic Boussinesq solves, comparing the CPU-only runtimes with the GPU runtimes for two different sets of Boussinesq runs distinguished by their resolutions (see legend), in the system with NVLink. Note, for fixed resolution and same number of cores, the significant gains when GPUs are used. As the figure is in log-log scale, the reference line with slope of  $-1$  indicates ideal scaling for which the time scales as  $1/N_c$  where  $N_c$  is the number of CPU cores.

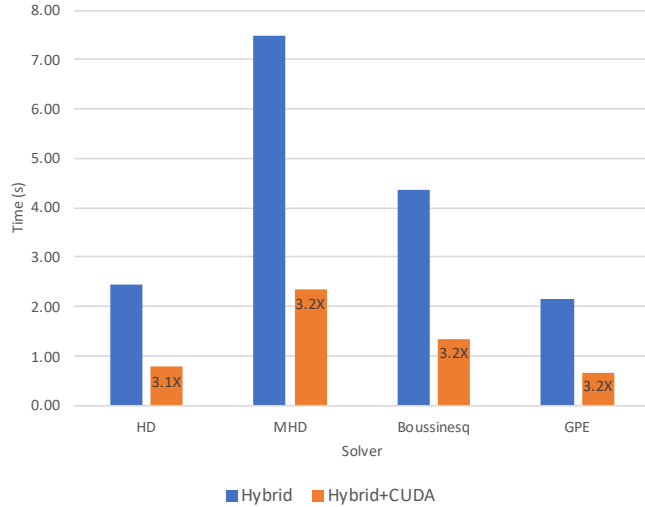


Figure 8: Bar plot of the total time per time step (for the full CFD code) in CPU-only and GPU runs for each of four solvers on an isotropic grid of  $512^3$  points with 4 nodes, 4 MPI tasks and GPUs per node, and 4 threads per MPI task. The speed-up of the GPU runs for each solver is indicated in the runtime bar for the GPU run.

when the GPU formulation is used. The average parallel efficiency based on the aggregate time is slightly greater than 1 (slight super scaling). The scaling is perhaps seen better in the more traditional scaling plot of Fig. 7, in which CPU-only and GPU total times are provided for Boussinesq runs at two different spatial resolutions ( $1024 \times 1024 \times 256$  and  $2048 \times 2048 \times 512$  grid points). The plot is in log-log scale, such that an ideal scaling for which the total time to perform a time step scales as the inverse of the number of cores,  $1/N_c$ , corresponds in this figure to a linear function with slope of  $-1$ . The simulations for the largest resolution in Fig. 7 are performed using up to 256 CPU cores, and up to the 256 CPU cores plus 64 GPUs when the GPU-based FFTs are used. It is clear from this figure that the scaling is nearly ideal on this system for all cases considered.

As a final comment, it is worth mentioning that we conducted a production run using a preliminary version of this code with the Boussinesq solver (Rosenberg et al., 2015) using the Titan supercomputer at Oak Ridge National Laboratory. Titan has 18688 nodes, each with one AMD Opteron 6274 CPU (with 16 cores per CPU) and an NVIDIA Tesla K20X GPU. Although the preliminary version of the code used in that system did not use streams, and had local transpositions done in the CPUs (and thus cannot be directly compared with the results presented here, as the observed speed for that preliminary version of the code was only of 1.7), we still observed good parallel scaling in a  $4096^3$  run up to  $10^5$  cores and 6250 GPUs (for more details, see Rosenberg et al., 2015).

#### 4.4. Behavior of different solvers

In the previous subsections we have shown that the the total runtime (and component process times) for the GPU implementation follow largely the CPU-only results in their strong scaling, when solving the Boussinesq equations (albeit the HD equations were also briefly considered). We expect that, as the number of nonlinear terms in the PDEs (or the number of primitive variables) is changed by a change of PDEs, the overall scaling will remain good for each PDE solver for both the CPU-only and GPU results, and we have verified this (not shown). We also expect that the speed-up in the runs with the CUDA transform over the hybrid runs for different PDEs will be similar to those in Sec. 4.3, another behavior that was verified by our tests. For the sake of brevity, here we summarize those studies by providing some actual measurements on the NVLink test system.

Fig. 8 shows the aggregate runtimes for four different solvers. Total times are provided for a CPU-only run and a GPU run in order to compare observed speed-ups. The solvers, HD (Mininni et al., 2008), MHD (Mininni and Pouquet, 2007), GPE (di Leoni et al., 2015), and Boussinesq (Rosenberg et al., 2015), have 3, 6, 1 complex (or 2 real), and 4 primitive fields, respectively, each solver requiring a number of distributed forward and backward transforms

per time step proportional to the number of nonlinear terms in the equations (and proportional to the number of fields). The node layout is the same as that in Sec. 4.3, and four nodes are used for each solver, each on a grid of  $512^3$  points. The measured speed-up of the GPU implementation of each solver over its CPU-only counterpart is indicated. All solvers see approximately the same speed-up of  $S_{\text{agg}} = 3.2$ , similar to the anisotropic Boussinesq runs above. It is clear that neither the number of distributed transforms nor the type of grid affects the aggregate speed-up on this system. This finding, together with the scaling (admittedly to small node counts) gives us strong confidence that we will see a convincing advantage in using the CUDA implementation in our production turbulence runs on forthcoming GPU-based systems.

## 5. Discussion and conclusion

We have built upon the hybrid MPI-OpenMP parallelization scheme presented in **M11** to add a third level of parallelization by developing a CUDA implementation of the Geophysical High Order Suite for Turbulence (GHOST) code’s distributed multi-dimensional Fourier transform. Whereas in **M11** an isotropic grid alone was considered, in this paper the tests admit grids with non-unit aspect ratio, a useful device for atmospheric and ocean turbulence studies. The method leverages the 1D coarse domain decomposition of the basic hybrid (CPU-only) scheme, and each MPI task now binds one GPU for additional fine grain parallelization. Our implementation hinges on the NVIDIA cuFFT advanced data layout library for device-capable local FFT routines, and depends considerably on the CUDA runtime to help manage data motion between the host and device. Implementation details have been provided that show how we have integrated the access to the CUDA runtime and cuFFT libraries into the code in a portable manner by using ISO bindings. We also explain how the additional parallelism leverages the existing hybrid (“CPU-only”) scheme, and may be useful for multicore systems that may have fewer GPUs than cores. The resulting method is portable and provides three levels of parallelization, allowing the usage by a high-order CFD code of all CPU cores and GPUs in a system, and providing typical speed-ups between 3 and 4 in tests with multiple GPUs.

Results have been presented that test the new hybrid/CUDA, GPU-based approach using, importantly, timings measuring the aggregate benefit of the implementation. As mentioned, we have demonstrated that the method can provide significant speed-up over the CPU-only computations with the addition of GPU-based computations of the distributed transform. We show that the speed-ups are reasonably consistent with heuristics when factoring in the performance enhancement afforded by threads for the primary costs in the transform. Aside from communication, which remains a major issue in a distributed transform like ours, device data transfer times can be a significant bottleneck with this method, but we have seen that NVIDIA’s NVLink effectively remedies this situation.

While we have seen that 80-90% of total runtime is spent on the distributed transform alone, the rest of the computations could in principle be placed on the device as well. One possibility is to use OpenACC (OpenACC Organization, 2018), which is a directive-based programming model that allows access to the offloading device with a rich set of features particularly for GPUs. While this, in principle, allows us to perform all computations on the GPU, there is a practical limit: Turbulence codes typically do quite a large amount of diagnostic, data-analytic, and restart output at different—but regular—intervals during a production run. Each of these output events requires that the CPU be engaged, so we must always be aware that data must be available on the host. Thus, we believe our three-level method combining CPU and GPU computations is particularly useful for massive CFD studies of turbulent flows.

While in our implementation we transfer data from the GPU back to the host in order to handle our all-to-all communication, GPUDirect<sup>TM</sup> (see Sec. 3.1) may even help incentivize migrating all computations to the GPU. GPUDirect<sup>TM</sup> enables the GPU to share (page-locked) memory with network devices without having to go through the CPU using an extra copy to host memory. This should, at a minimum, reduce communication latency, and may prove to be an important future path.

We have concentrated on the CUDA stream implementation in this version as a way to overlap data transfer with computation of the cuFFTs. In general we see a benefit on runtimes of about 30% when using PCIe, but that this benefit is reduced when using NVLink. We have not explored whether zero-copy access of the data by the CUDA kernels can provide a larger gain when using PCIe. Since we are already using the page-locked host memory, it may be possible to see still more improved transfer speeds using zero-copy access with the CUDA Unified Memory model (NVIDIA, 2018c), but with the sizeable improvement offered by NVLink it seems a questionable investment. On the other hand, Unified Memory also offers the potential to clean up the data management code presented in this work considerably. We have begun such an implementation and will report on it in the future.



## 6. Acknowledgements

Computer time was provided by NSF under sponsorship of the National Center for Atmospheric Research and is gratefully acknowledged. This research also used resources of the Oak Ridge Leadership Computing Facility, which is a DOE Office of Science User Facility supported under Contract DE-AC05-00OR22725. Support for AP from LASP and, in particular, from Bob Ergun, is gratefully acknowledged.

## References

- Canuto, C., Hussaini, M. Y., Quateroni, A., Zang, T. A., 1988. *Spectral Methods in Fluid Dynamics*. Springer (New York).
- Chatterjee, A. G., Verma, M. K., Kumarand, A., Samtaney, R., Hadri, B., Khurram, R., 2018. Scaling of a Fast Fourier Transform and a pseudo-spectral fluid solver up to 196608 cores. *J. Parallel Distrib. Comput.* 113, 77 – 91.
- di Leoni, P. C., Mininni, P. D., Brachet, M. E., 2015. Spatiotemporal detection of Kelvin waves in quantum turbulence simulations. *Phys. Rev. A* 92, 063632.
- Dmitruk, P., Wang, L.-P., Matthaeus, W. H., Zhang, R., Seckel, D., 2001. Scalable parallel FFT for simulations on a Beowulf cluster. *Parallel Computing* 27, 1921–1936.
- Donzis, D. A., Yeung, P. K., Pekurovsky, D., 2008. Turbulence simulations at  $O(10^4)$  core counts. In: TeraGrid '08 Conference, Las Vegas, NV. Science track paper.
- Frigo, M., Johnson, S. G., 1998. The design and implementation of FFTW. In: *Proc. IEEE Intl. Conf. Acoustics Speech and Signal Processing*. Vol. 3. p. 1381.
- Frigo, M., Johnson, S. G., 2005. The design and implementation of FFTW3. In: *Proceedings of the IEEE*. Vol. 93. New York, Academic Press, Inc, pp. 216–231.
- Gómez, D. O., Mininni, P. D., Dmitruk, P., 2005. Parallel simulations in turbulent MHD. *Physica Scripta T116*, 123–127.
- Gottlieb, D., Hussaini, M. Y., Orszag, S. A., 1984. *Spectral Methods for Partial Differential Equations*. SIAM, Philadelphia.
- Govett, M., Rosinski, J., Middlecoff, J., Henderson, T., Lee, J., MacDonald, A., Wang, N., Madden, P., Schran, J., Duarte, A., 2017. Parallelization and performance of the NIM Weather Model on CPU, GPU, and MIC processors. *Bull. Am. Meteorol. Soc.* 98 (10), 2201 – 2213.
- Kaneda, T., Ishihara, Yokokawa, M., Itakura, K., Uno, A., 2003. Energy dissipation rate and energy spectrum in high-resolution DNS of turbulence in a periodic box. *Phys. Fluids* 15, L21–L24.
- Mininni, P., Alexakis, A., Pouquet, A., 2008. Nonlocal interactions in hydrodynamic turbulence at high Reynolds numbers: The slow emergence of scaling laws. *Phys. Rev. E* 77, 036306.
- Mininni, P., Rosenberg, D., Reddy, R., Pouquet, A., 2011. A hybrid MPI-OpenMP scheme for scalable parallel pseudospectral computations for fluid turbulence. *Parallel Computing* 37, 316–326.
- Mininni, P. D., Pouquet, A., 2007. Energy spectra stemming from interactions of Alfvén waves and turbulent eddies. *Phys. Rev. Lett.* 99, 254502.
- NVIDIA, 2018a. CUDA runtime API. <http://docs.nvidia.com/cuda/cuda-runtime-api/index.html>, version v9.2.148, accessed: 2018-07-26.
- NVIDIA, 2018b. cuFFT development. <https://developer.nvidia.com/cufft>, accessed: 2018-03-14.
- NVIDIA, 2018c. NVIDIA Unified Memory. <https://devblogs.nvidia.com/maximizing-unified-memory-performance-cuda>, accessed: 2018-03-14.
- OpenACC Organization, 2018. OpenACC. <https://www.openacc.org/>, accessed: 2018-03-14.
- Orszag, S. A., 1972. Comparison of pseudospectral and spectral approximation. *Stud. Appl. Math.* 51, 253–259.
- Patterson, G., Orszag, S. A., 1971. Spectral calculations of isotropic turbulence: efficient removal of aliasing interactions. *Phys. Fluids* 14, 2538–2541.
- Ripesi, P., Biferale, L., Schifano, S., Tripiccion, R., 2014. Evolution of a double-front rayleigh-taylor system using a graphics-processing-unit-based high-resolution thermal lattice-boltzmann model. *Phys. Rev. E* 89, 043022.
- Rosenberg, D., Pouquet, A., Marino, R., Mininni, P. D., 2015. Evidence for Bolgiano-Obukhov scaling in rotating stratified turbulence using high-resolution direct numerical simulations. *Phys. Fluids* 27, 055105.
- Sanders, J., Kandrot, E., 2011. *CUDA By Example*. Addison-Wesley.
- Sojovolosky, N. E., Mininni, P. D., Pouquet, A., 2018. Generation of turbulence through frontogenesis in sheared stratified flows. *arXiv* 1708.10287.
- Stürmer, M., Götz, J., Richter, G., Dörfler, A., Rude, U., 2009. Fluid flow simulation on the Cell Broadband Engine using the lattice Boltzmann method. *Comput. Math Appl.* 58, 1062 – 1070.
- Thibault, J. C., Senocak, I., 2009. CUDA Implementation of a Navier-Stokes solver on multi-GPU desktop platforms for incompressible flows.
- Yeung, P., Donzis, D., Sreenivasan, K., 2005. High Reynolds number simulation of turbulent mixing. *Phys. Fluids* 17, 081703.
- Yokota, R., L.A.Barba, Narumiand, T., Yasuoka, K., 2013. Petascale turbulence simulation using a highly parallel fast multipole method on GPUs. *Comp. Phys. Comm.* 184, 445 – 455.